Research Article

Klaudia Żebrowska, Małgorzata Grabowska, Emerson Coy, Katarzyna Rolle, Radosław Mrówczyński*, and Bartosz F. Grześkowiak*

In vitro anticancer activity of melanin-like nanoparticles for multimodal therapy of glioblastoma

https://doi.org/10.1515/ntrev-2023-0206
received November 8, 2023; accepted January 23, 2024

Abstract: Glioblastoma (GBM) is one of the most aggressive and hard to treat cancers. Traditional anti-cancer treatment methods have low efficiency and the lifespan after diagnosis is only 12–18 months. Brain tumor cells overexpress many proteins that play an important role in tumor progression and can be used as therapeutic targets. One of the promising approaches in cancer treatment is down-regulation of an extracellular matrix glycoprotein – Tenascin-C (TN-C) through RNA interference therapy. However, the effective delivery of double stranded RNA with one strand complementary to TN-C mRNA sequence is difficult due to rapid degradation by nucleases and low intracellular uptake. Polydopamine (PDA), a biomimetic polymer characterized by high biocompatibility and simple modification ability, is commonly used in nanobiomedicine to create a drug/gene delivery vehicle. Furthermore, photothermal characteristics of this polymer enable its application in photothermal therapy (PTT), which is a great option for cancer treatment. Here we synthesize PDA nanoparticles (NPs) coated with polyamidoamine dendrimers generation 3.0 (DD3.0) for therapeutic anti-TN-C RNA and doxorubicin delivery. As prepared PDA@DD3.0 NPs are then used in combined drug delivery, gene silencing, and PTT of GBM. The obtained materials are analyzed in terms of physicochemical and photothermal properties as well as their cytotoxicity, using human GBM cells. The results demonstrate that the obtained nanocarriers are effective non-viral vehicle for combined therapeutic approach for killing glioma cells *via* anti-TN-C RNA delivery and combined chemo-PTT therapy (CT-PTT). The application of PDA@DD3.0 NPs contributed to the 3-fold reduction in the proliferation rate of GBM cells, a decrease in the level of TN-C expression (by 30%) and a reduction in the number of viable cells by up to 20%.

Keywords: polydopamine, nanoparticles, glioblastoma, combined therapy, photothermal therapy, gene therapy

*** Corresponding author: Radosław Mrówczyński,** Faculty of Chemistry, Adam Mickiewicz University in Poznań, Uniwersytetu Poznańskiego 8, 61-614 Poznań, Poland; Centre for Advanced Technologies, Adam Mickiewicz University in Poznań, Uniwersytetu Poznańskiego 10, 61-614 Poznań, Poland,
e-mail: radoslaw.mrowczynski@amu.edu.pl
*** Corresponding author: Bartosz F. Grześkowiak,** NanoBioMedical Centre, Adam Mickiewicz University in Poznań, Wszechnicy Piastowskiej 3, 61-614 Poznań, Poland, e-mail: bartoszg@amu.edu.pl
Klaudia Żebrowska, **Emerson Coy:** NanoBioMedical Centre, Adam Mickiewicz University in Poznań, Wszechnicy Piastowskiej 3, 61-614 Poznań, Poland
Małgorzata Grabowska: Institute of Molecular Biology and Biotechnology, Faculty of Biology, Adam Mickiewicz University in Poznań, Uniwersytetu Poznańskiego 6, 61-614 Poznań, Poland
Katarzyna Rolle: Department of Molecular Neurooncology, Institute of Bioorganic Chemistry of the Polish Academy of Sciences, Noskowskiego 12/14, 61-704 Poznań, Poland

1 Introduction

Glioblastoma (GBM) is the most commonly occurring high-grade primary malignant brain tumor with very poor prognosis [1,2]. Taking into account that currently approved treatments for GBM are characterized by the low survival rate, new therapeutic strategies are urgently needed. Despite advances in neurosurgery, chemotherapy, and radiotherapy, GBM remains one of the most treatment-resistant central nervous system malignancies with an average survival time of approximately 15 months, and a 5-year survival rate of only 5% [3]. Moreover, what makes GBM therapy truly complex is: (i) tumor location and heterogeneity make its resection difficult; (ii) resistance to gold standard temozolomide (TMZ) treatment, mostly due to over-expression of O^6-methylguanine-DNA methyltransferase which limits the cytotoxic effects of TMZ; and (iii) inability of chemotherapeutics to cross blood-brain-barriers (BBB) [2,4–7]. Together with the development of nanotechnology, nanoparticles (NPs) have been proposed as materials for preparation of a new drug delivery systems that are supposed to improve the therapeutic outcome in oncological

diseases and enhanced patient life quality during treatment. The success of nanomaterials application in medicine (nanomedicine) has been determined by their versatility and ability to overcome some of the critical limitations of conventional drugs such as the inability to cross the biological barriers, poor accumulation at the targeted brain tumor site, and high systemic side effects [8–13].

There are several requirements for nanocarriers to be used in drug delivery to GBM. First of all, the particles should be biocompatible and not harm healthy cells. Second, the particle size should be below 200 nm so as not to cause physical damage to the BBB and surrounding tissues. Finally, the particles should rather exhibit positive charge to interact with BBB, but the charge cannot be too high, otherwise the carriers can be toxic [14]. Indeed, different nanostructure types have been used to prepare drug delivery systems capable of providing chemotherapeutics to GBM [15–17]. The most common materials include poly(lactic-*co*-glycolic acid), micelles, magnetic NPs, and dendrimers. In addition to cytostatic drugs, the latest nanomaterials enable the delivery of genetic materials including dsRNA or siRNA to knock down genes responsible for appropriate protein expression in GBM growth and migration *via* the RNA interference (RNAi) strategy [18–25]. Among the proteins that have become a target for GBM treatment, Tenascin-C (TN-C) has drawn considerable attention of many scientific groups. TN-C is a large extracellular matrix glycoprotein with a mass of about 180–250 kDa as an intact monomer and up to 1,800 kDa when assembled into a hexamer [26]. In normal adult tissue, TN-C expression is mainly restricted to the bone marrow, thymus, spleen, and lymph nodes, especially in T-lymphocyte-dependent zones [27]. However, TN-C has been reported to play a role in tumor-induced immunosuppression, because it is highly expressed in most solid tumors, including those arising in the breast, uterus, ovaries, prostate, pancreas, colon, stomach, mouth, larynx, lung, liver, kidney, bladder, skin, bone, soft tissues, and lymphomas [28]. Many reports suggest an important role of TN-C in tumor growth, metastasis, tumor angiogenesis, and inhibition of immune surveillance. Furthermore, it has been reported that TN-C, an extracellular matrix protein, is highly expressed in the tumor tissue of most malignancies, including the brain [29–32]. Importantly, elevated TN-C level in high-grade gliomas increases the invasiveness of glioma cells by promoting endothelial cell migration [33,34]. Therefore, TN-C is the dominant GBM epitope. However, the clinical application of RNAi-based therapeutics, including dsRNA/siRNA, is limited due to their susceptibility to intravascular degradation and lack of tissue-penetrating ability. The solution to this drawback was the use of magnetic NPs with polyetyleneimine (PEI), which acted as an effective drug carrier of dsRNA with a sequence complementary to TN-C, preventing its degradation and ensuring not only significant TN-C expression level suppression, but also impairing migration of the tumor cells [25].

Further progress in nanotechnology have resulted in the development of materials capable of co-delivery of chemotherapeutic agents and nucleic acids for GBM treatment [35–37]. So far, several research groups have reported the synergistic effects of this approach. For example, co-delivery of doxorubicin (DOX) and siRNA using a generation-3 (G3) poly(L-lysine) OAS dendrimers to U-87 GBM cells has been shown to result in significantly high gene silencing in U87-Luc cells due to the combined effects of cytotoxicity and RNAi activity [38]. Polymeric NPs made of PEI and polycaprolactone were also used to deliver DOX and siRNA downregulating BCl-2 and upregulating BAX to C6 rat glioma cells [39].

Another important therapeutic approach in cancer treatment using NPs is photothermal therapy (PTT) [40–44]. In this strategy, nanomaterials are applied as smart nanophotothermal agents to convert light into heat, which generates hyperthermia inside cancer cells leading to their death. The most common light source is near-infrared (NIR) laser beam that operates in the range of 650–1,000 nm. This region is called the "I biological window," in which light has the maximum depth of penetration into the tissue and is not disturbed by water absorption, which takes place at a longer wavelength. On the other hand, light is also one of the promising triggering mechanisms used as external stimuli to trigger drug release from the photo-responsive nanocarriers. The NIR light-responsivity of nanomaterials enables on-demand elevated drug release in cancer photo-chemotherapy [45,46]. The PTT belongs to rapidly emerging areas of NPs-based GBM treatment.

There is an urgent need to synthesize nanocarriers for cancer therapy capable of combining different modalities in a single nanoplatform, as these materials appear to have advantages over lower-generation materials allowing the application of only single modality. Indeed, combined chemo- and PTT is a newly explored route in GBM treatment, which can be used to eradicate glioma cells. For this purpose, materials for the preparation of nanocarriers should be carefully selected, as the material itself may provide the desired feature, *e.g.*, photothermal properties. Polydopamine (PDA) is an excellent example of a material that, due to its versatility, has found application in the synthesis of multifunctional nanostructures for oncology [11,47–52]. This substance structurally resembles the naturally occurring black pigment in the human body and other animals. It exhibits strong adhesive properties, often comparable to those of mussels [53,54]. What makes PDA a suitable material for preparing hybrid nanostructures for

cancer treatment is its proven biocompatibility, simple surface functionalization with amines, thiols, or *via* ring opening polymerization, one of the highest values of photothermal conversion efficiency and relatively good absorption in the first biological window. Thus, PDA-based hybrid materials with access to multiple "functions" are considered "game changer" in the field of NPs for oncological purposes [55–57].

Recent reports show that hybrid materials composed of polyamidoamine (PAMAM) dendrimers coated PDA NPs (PDA@PAMAM) can be used as carriers for combined chemo- and PTT of liver cancer [58]. Moreover, the merging of PAMAM dendrimers with PDA and magnetic NPs led to the creation of multifunctional NPs capable of killing cancer cells while maintaining MRI contrast properties [59]. Combining PDA with nanodiamonds resulted in successful removal of glioma cells, while the nanodiamonds retained their fluorescent tracking properties [60,61]. Recently, the application of PDA-based nanostructures in GBM therapy has been extensively reviewed [62]. The gathered results indicate that indeed PDA-based materials are either used in PTT or drug delivery only, while their application in combined modalities, including RNAi, remains an unexplored area.

Here we present the application of PDA@PAMAM hybrid material that meets all the key requirements, such as biocompatibility, positive zeta potential, size below 200 nm, and strong photothermal properties, to be used in GBM therapy. The presented platform can encapsulate a chemotherapeutic drug and additionally has the ability to bind and deliver dsRNA, which makes the carrier suitable for photothermal, gene-, and chemotherapy (Figure 1). Our results demonstrate a new path in the development of PDA-based materials for GBM therapy, meeting the requirements of modern multifunctional nanostructures.

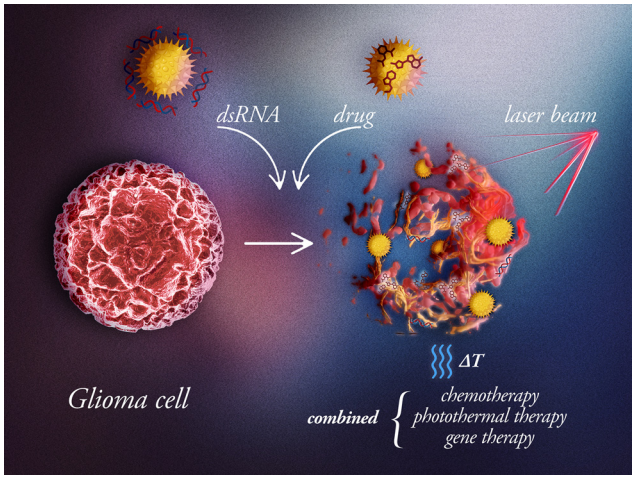

Figure 1: Schematic presentation of PDA@DD3.0 nanocarrier application in combined chemo-, photo-, and gene therapy of GBM cells.

2 Materials and methods

2.1 Reagents and cells

Dopamine hydrochloride (purity: 99%, MW: 189.64) was acquired from Alfa Aesar (Poland). DOX and hydrochloride salt were obtained from LC Laboratories (USA). PAMAM dendrimers G 3.0, tris(hydroxymethyl) aminomethane (TRIS) tablets, Triton X-100, fetal bovine serum (FBS), penicillin 100 U/mL, streptomycin 100 µg/mL, MUSE® count and viability kit, WST-1 cell proliferation kit, and Transcriptor High Fidelity complementary DNA (cDNA) synthesis kit were acquired from Merck Millipore (USA). Dulbecco's Modified Eagle's Medium (DMEM), Calcein AM, ethidium homodimer-2 (EthD-2), formaldehyde, Trizol, Hoechst 33342, Dulbecco's phosphate-buffered saline with and without Ca^{2+} and Mg^{2+}, and DNA-free DNA removal kit were obtained from Thermo Fisher Scientific (USA). ClickTech EdU cell proliferation assay was purchased from Baseclick GmbH (Germany).

The GBM multiforme-derived human U-118 MG cell line as well as human fibroblast MRC-5 cell line were obtained from the American Type Culture Collection (ATCC, USA). Cells were maintained in DMEM supplemented with 10% FBS and 1% antibiotics (penicillin 100 U/mL, streptomycin 100 µg/mL) under standard conditions (37°C, 5% CO_2).

2.2 Synthesis and functionalization of PDA NPs with PAMAM dendrimers G 3.0

200 mg dopamine hydrochloride dissolved in 100 mL of Milli-Q water in a round-bottom flask was placed on a magnetic stirrer and heated up to 50°C. Then, different volumes of 1M NaOH solution (0.8, 0.7, 0.5, 0.2) were added at 48°C. After 3 h of mixing, the particles were collected and purified by centrifugation (22,000 rpm, 20 min) and washed three times with Milli-Q water. To functionalize the NPs, 10 mg of PDA NPs were added to 30 mL of 10 mM TRIS buffer (pH 8.5) in a locked flat bottom flask. The solution was sonicated and placed on a magnetic stirrer. During the mixing, 213.6 µL of PAMAM dendrimers G 3.0 were slowly dropped into the solution at room temperature (RT). After overnight incubation, the particles were collected by centrifugation (22,000 rpm, 15 min) and washed three times with Milli-Q water. The obtained NPs were hereafter referred to as PDA@DD3.0.

2.3 Characterization of dendrimer coated PDA NPs

The electrokinetic potentials of PDA NPs were measured using Malvern Zetasizer Nano-ZS Dynamic Light Scattering Analyzer (Malvern Instruments Ltd., Malvern, UK). The dispersion status and morphology of the samples were visualized with high-resolution transmission electron microscopy (HRTEM; JEM-ARM200F, JEOL, Tokyo, Japan). Fourier-transform infrared spectroscopy (FTIR) of the materials was carried out on a Bruker Tensor II (Bruker, Germany) spectrometer. The NPs were dried, ground with KBr, and pressed into a pellet.

2.4 Photothermal measurements

Photothermal measurements were conducted in a 1 cm square quartz cuvette with a 10 mm optical path length (high precision Quartz SUPRASIL cell [Hellma Analytics]). The distance between the laser and the cuvette was 10 cm. Various concentrations of PDA NPs ranging from 5 to 100 μg/mL were prepared in a total volume of 1 mL of water. Water was used as a control sample. To avoid sedimentation of NPs, the solution was constantly mixed during the experiment. The temperature was recorded at 10 s intervals over 10 min of irradiation with 808 nm wavelength laser light (Changchun New Industries Optoelectronics Tech. Co., Ltd, China) and laser power of 3 W. The photostability of PDA NPs with a concentration of 50 μg/mL was measured in five on/off irradiation cycles for 5 min The temperature of the solutions was recorded by a digital thermometer with a thermocouple sensor and thermal camera. Thermal imaging was conducted using KT-650 thermal camera (SONEL, Poland).

2.5 DOX loading and release

1 mg of PDA@DD3.0 was dispersed in 1 mL of PBS buffer (pH 7.5) containing DOX at a concentration of 1 mg/mL and constantly mixed in a thermal shaker at 25°C for 24 h. Then, the particles were collected by centrifugation (13,400 rpm, 4 min) and purified with PBS buffer to achieve a clear solution. After each centrifugation step, the PBS buffer was collected and analyzed by UV-Vis spectroscopy. All measurements were conducted in triplicate. The achieved NPs are hereafter referred to as PDA@DD3.0@DOX.

The encapsulation efficiency (EE%) and loading capacity (LC%) were calculated according to following formulas, respectively:

$$\mathrm{EE\%} = \frac{\text{Total mass of added drug} - \text{Mass of free non entrapted drug}}{\text{Total mass of added drug}} \times 100\%,$$

$$\mathrm{LC\%} = \frac{\text{Mass of entraped drug in nanoparticles}}{\text{Mass of nanoparticles}} \times 100\%.$$

The DOX release from the PDA@DD3.0@DOX sample was examined in three different buffers: citric acid (CA) buffer at pH 4.5 and pH 5.5, and PBS buffer at pH 7.5. 1 mg of NPs was dispersed in 1 mL of appropriate solutions with different pH and placed in a thermal shaker at 37°C (human body temperature) for 1, 2, 3, 4, 5, 6, 24, and 48 h. Next the particles were collected at given time intervals by centrifugation (13,400 rpm, 4 min) and supernatant was analyzed by UV-Vis spectroscopy. All measurements were conducted in triplicate.

2.6 Attachment of dsRNA

1 μg of double-stranded RNA (dsRNA) with a length of 163 nucleotides and a sequence complementary to mRNA of TN-C (ATN-RNA) (US Patent US 8946400 B2) was complexed with a series of PDA@DD3.0 or PDA@DD3.0@DOX weight ratios (1:1, 5:1, 10:1, 15:1, 20:1, and 30:1 NPs to RNA wt/wt ratio) in 50 μL of water and incubated for 30 min in RT. For biological assays, the water was replaced with Opti-MEM medium. The electrophoretic separation was conducted at 70 V for 20 min. The gel was then visualized under UV light in a transilluminator.

2.7 Cell viability assays

2.7.1 WST-1 cell proliferation assay

WST-1 cell proliferation assay (Clontech, USA) was conducted to evaluate the cytotoxicity of NPs. The WST-1 cell proliferation assay involves the enzymatic cleavage of the tetrazolium salt WST-1 to a water-soluble formazan dye by living cells, which can be determined by measuring absorbance at 420–480 nm. U-118 MG and MRC-5 cells were seeded at a density of 8×10^3 and 5×10^3 cells per well, respectively, in a 96-well plate for 24 h. Then, the increasing concentrations of tested NPs (1.125, 2.5, 5,

10 μg/mL) were added to each well, and the cells were incubated for another 48 h. Next 10 μL of the WST-1 cell proliferation reagent was added to each well and incubated for 4 h. Finally, 100 μL of the medium was transferred to new wells and the absorbance was recorded at 450 nm (reference wavelength 620 nm) against the background control, using an Anthos Zenyth 340rt multiwell-plate reader (Biochrom, UK). The cell viability was expressed as the respiration activity normalized to untreated cells. All experiments were carried out in triplicate.

2.7.2 Live/dead assay

After 48 h incubation of cells with NPs, 100 μL of a dye mixture containing 2 μM calcein, 2 μM EthD, and 8 μM Hoechst 33342 in PBS buffer was added per well for 30 min at 37°C. Next the analysis was conducted using the In Cell Analyzer 2000 bioimager. Live cells were visualized using a green emission filter (FITC), dead cells with a red emission filter (TexasRed), and DAPI filter was used to image the blue signal of the nucleus. Image acquisition of 20 randomly selected fields within one well were performed at 20× magnification. Evaluation of archived images was carried out using the IN Cell Developer Toolbox software. DAPI channel images determined the total number of cells. The number of live cells was established from images in the FITC channel, while images in the TexasRed channel determined the number of dead cells.

2.7.3 EdU cell proliferation assay

To differentiate between cells that are actively dividing and those that are quiescent after incubation with PDA@DD3.0@DOX NPs, the ClickTech EdU cell proliferation assay was performed. In this test, the modified thymidine analogue EdU is effectively built into newly synthesized DNA and fluorescently labeled with a bright, photostable Eterneon-Red 645 dye azide in a rapid, highly specific click reaction. Briefly, 100 μL of 2× EdU working solution containing 5-ethynyl-deoxyuridine (5-EdU) was added to the well containing 100 μL of cell medium and incubated for 24 h. After this time, the cells were fixed with 4% formaldehyde solution and permeabilized with 0.5% Triton X-100. Next the permeabilization solution was removed and the reaction cocktail containing Eterneon-Red 645 Azide was added for 30 min to detect EdU. Additionally, the cell nuclei were labeled with 8 μM Hoechst 33342. The cells were imaged using the IN Cell Analyzer 2000. Proliferating cells were imaged using the Cy5/Cy5 ex/em filters while the DAPI/DAPI ex/em filters were applied for all cells. Twenty fields of view were taken per well with a 20× magnification. The obtained images were evaluated using the IN Cell Developer Toolbox software (GE Healthcare Life Sciences) using an in-house developed protocol. In the first step, the total cell number was calculated from the DAPI images. Finally, the number of proliferating cells from the Cy5 images was established.

2.7.4 Viability assay after PTT

In order to evaluate the efficacy of the achieved materials in PTT after NIR irradiation, U-118 MG cells were seeded at a density of 8×10^3 cells per well in 96-well plates. Next the cells were incubated with an increasing (1.125, 2.5, 5, and 10 μg/mL) concentration of NPs. After 24 h, the cells were irradiated with a laser with a wavelength of 808 nm and a power of 3 W for 5 min. The cells were then incubated for another 24 h and flow cytometric analysis using the MUSE® count and viability kit was conducted. In the MUSE® count and viability assay, both viable and nonviable cells were stained differentially based on their permeability to the DNA-binding dyes. Briefly, cells were trypsinized and transferred to 1.5 mL centrifuge tube. Due to observed detachment of the cells upon laser irradiation, supernatant as well as PBS buffer used for washing of cells were transferred to the same tube. The resulting mixture was centrifuged for 5 min at 1,200 rpm and the supernatant was discarded. The sediment was washed with PBS and centrifuged under the same conditions. In the end, cells were suspended in 10 μL of PBS and mixed with 190 μL of the MUSE® count and viability reagent, followed by 10 min incubation at RT in the dark. The stained cells were examined using the MUSE® cell analyzer (Merck Millipore). Non-irradiated cells incubated with NPs were used as a control.

To image live and dead cells, U-118 MG cells seeded at the density of 8×10^3 cells per well in 96-well plate were incubated with an increasing (1.125, 2.5, 5, and 10 μg/mL) concentration of NPs. After 24 h, the cells were irradiated with 808 nm laser with a power of 3 W for 5 min. 24 h later, the cells were stained with 2 μM calcein AM and 2 μM EthD-2 containing PBS (100 μL/well) for 30 min at 37°C. Eventually, the cells were visualized with the IN Cell Analyzer 2000 (GE Healthcare Life Sciences, USA). Live cells were imaged using a green emission filter (FITC), while the dead cells were visualized with a red emission filter (TexasRed).

2.8 mRNA expression measurements

Total RNA was isolated from cell lines with TRIZOL reagent. RNA was then purified from residual DNA using a DNA-free

DNA Removal Kit according to the manufacturer's instructions. The procedure ended with analysis of the quantity and quality of the resulting RNA solution. The RNA concentration was determined spectrophotometrically at a wavelength of λ = 260 nm using Nano-Drop 2000. The degree of possible degradation of the material was checked by electrophoretic separation in a 1% agarose gel. The purified RNA was a template for the synthesis of cDNA. Reverse transcription was conducted using 500 ng of material with the Transcriptor High Fidelity cDNA Synthesis Kit according to the manufacturer's procedure.

The expression level of TN-C mRNA was tested by quantitative real-time PCR (qRT-PCR) using the CFX96 thermocycler (BioRad). The following primer sequences were used: TNC_L CCGGACCAAAACCATCAGT; TNC_R GGGATTAA TGTCGGAAATGGT. The qRT-PCR was conducted under the following conditions: an initial 5 min preincubation at 95°C, 45 cycles of denaturation in 95°C for 10 s, annealing at 55°C for 30 s, and extension at 72°C for 10 s. Hypoxanthine phosphoribosyltransferase (HPRT) was used as the endogenous control. Primer sequences were: HPRT_L TGACCTTGATTT ATTTTGCATACC; HPRT_R CGAGCAAGACGTTCAGTCCT. The CFX Maestro software allowed for an analysis of expression level using delta Ct method.

2.9 Cellular uptake

To image uptake of DOX, U-118 MG cells were plated at the density of 2.5 × 10^4 cells/well onto an 8-well Nunc® Lab-Tek® Chamber Slide (Thermo Fischer Scientific) and cultured for 24 h. Then, 50 µL of the sample at the concentration of 9 µg/mL per well was added and cells were incubated for 4 h. Next the cells were fixed with 4% formaldehyde in PBS buffer for 15 min. The cell nuclei were labeled with Hoechst 33342 at a concentration of 8 µM. Cells were visualized using a confocal laser scanning microscope (Olympus FV1000, Japan). Image acquisition and analysis were carried out with a 60× objective, a 1.4 oil immersion lens, and FV10-ASW software (Olympus). DOX fluorescence was detected using 488 nm excitation and 560–590 nm emission filters. The Hoechst 33342 fluorescence was visualized using 405 nm excitation source and 425–475 nm emission filters.

2.10 Statistical analysis

All experiments were conducted in triplicate and the results are presented as mean values ± standard deviation. Differences between mean values of the tested samples and controls were compared using analysis of variance extended with post-hoc Tukey or Bonferroni tests. Statistically significant results were achieved at the level of: * for $p < 0.05$; ** for $p < 0.01$; *** for $p < 0.001$; no statistical significance for $p \geq 0.05$.

3 Results and discussion

3.1 PDA NPs functionalization and characterization

The PDA NPs were synthesized by oxidative polymerization of dopamine hydrochloride under alkaline conditions according to a previously reported protocol [63]. The most important factors affecting the size of the PDA NPs during the synthesis process involve NaOH concentration, dopamine concentration, polymerization temperature, and the mixing time. In this study, different NaOH concentrations in the solution were added to manipulate the size of NPs whereas other parameters were kept constant. The particles obtained under different conditions were imaged by TEM. We demonstrated the relation between the amount of NaOH used and the size of NPs. A higher concentration of NaOH in the solution resulted in a smaller NPs diameter and more homogeneous sample. As shown in Figure 2a, the addition of 0.8 mL of NaOH resulted in population of particles with the size of 80 ± 18 nm in diameter while after adding 0.7 mL of NaOH, we obtained PDA NPs of size 92 ± 8 nm (Figure 2b). The synthesis performed with smaller volumes of NaOH resulted in achieving fractions of smaller and bigger NPs (Figure 2c and d). TEM investigation also demonstrated differences in the shape of PDA NPs. As the particle size increases, the shape of NPs becomes more defined and their surface is clearer and smoother. Moreover, their shape is not ideally spherical, and a large deviation in the NP sizes is apparent. As the size decreases, the surface of the particles became rougher, but they are still spherical in shape.

Well-defined PDA NPs with a size of 92 ± 8 nm in diameter were chosen for further steps to develop the multifunctional carrier. The structure of PDA particles was investigated by FTIR. The data obtained were consistent with those reported in the literature. As shown in Figure 2e, a large signal corresponding to the stretching vibrations of hydroxyl (−OH) and amine (N–H) groups, due to the hydroxyl and amine groups in the PDA structure, is visible in a range of 3,700–2,500 cm^{-1}, and the maximum value is about 3,400 cm^{-1}. The bending vibration of N–H bond was determined to be 1,628 cm^{-1} and

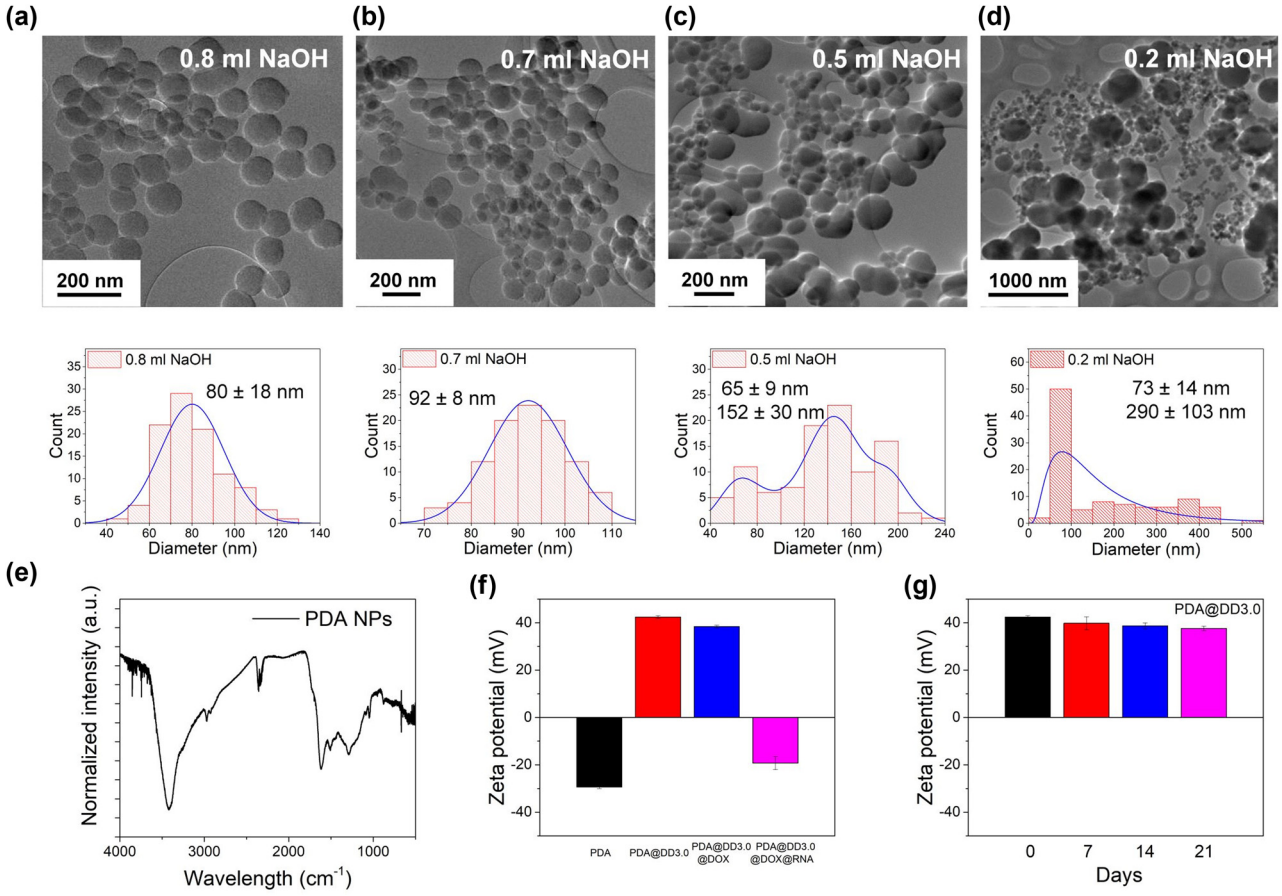

Figure 2: TEM images and histograms of PDA particles after synthesis with the addition of (a) 0.8 mL, (b) 0.7 mL, (c) 0.5 mL and (d) 0.2 mL NaOH; (e) FT-IR spectrum of PDA particles; (f) zeta potential value of PDA particles before and after functionalization with PAMAM dendrimers and loaded with DOX and RNA; and (g) stability of PDA@DD3.0 in time.

was assigned to the vibration of primary and secondary amine groups. The peak at 1,290 cm^{-1} indicates the presence of a C–O bond, while the signal at 1,472 cm^{-1} is attributed to the C═C ring stretching band overlapping with the $-CH_2$ scissoring band. Next PDA NPs underwent reaction with PAMAM dendrimers generation 3.0 (DD3.0). The selected dendrimers are characterized by a diameter of 3.2 nm and 32 surface amine group and ethylenediamine core. The dendrimers were connected to the PDA NPs surfaces *via* a Michael reaction between the peripheral amine groups present in DD3.0 and the quinone groups in the PDA structure [58,59,64]. We linked PDA particles to dendrimers to ensure high drug loading capacity and the positive zeta potential for further dsRNA binding. To confirm the efficacy of functionalization of PDA NPs, zeta potential measurements were conducted. The surface charge of mere PDA NPs was approximately –30 mV. This result was in agreement with literature reports showing the zeta potential value for mere PDA particles in a range between −4.58 and −39 mV [65–69]. The surface charge of PDA particles after functionalization with PAMAM dendrimers was enhanced to +44 mV due to the presence of amine group in the PAMAM structure (Figure 2f). These results clearly indicate that PAMAM dendrimers were linked to the surface of NPs. Next the stability of PDA@DD3.0 in time was assessed. We found out that obtained material PDA@DD3.0 remains stable in water for at least 21 days since we did not observe the changes in zeta potential value (Figure 2g).

3.2 Cytotoxicity of PDA NPs

In order to assess the effect of PDA@DD3.0 on the viability of U-118 MG GBM cells, WST-1 and live/dead assays were carried out as complementary methods. The same tests were performed on MRC-5 fibroblasts to evaluate the influence of the carrier on proliferation of normal cells. The WST-1 assay results reveal a slight decrease in cell viability of both cell types at the highest PDA@DD3.0 concentration.

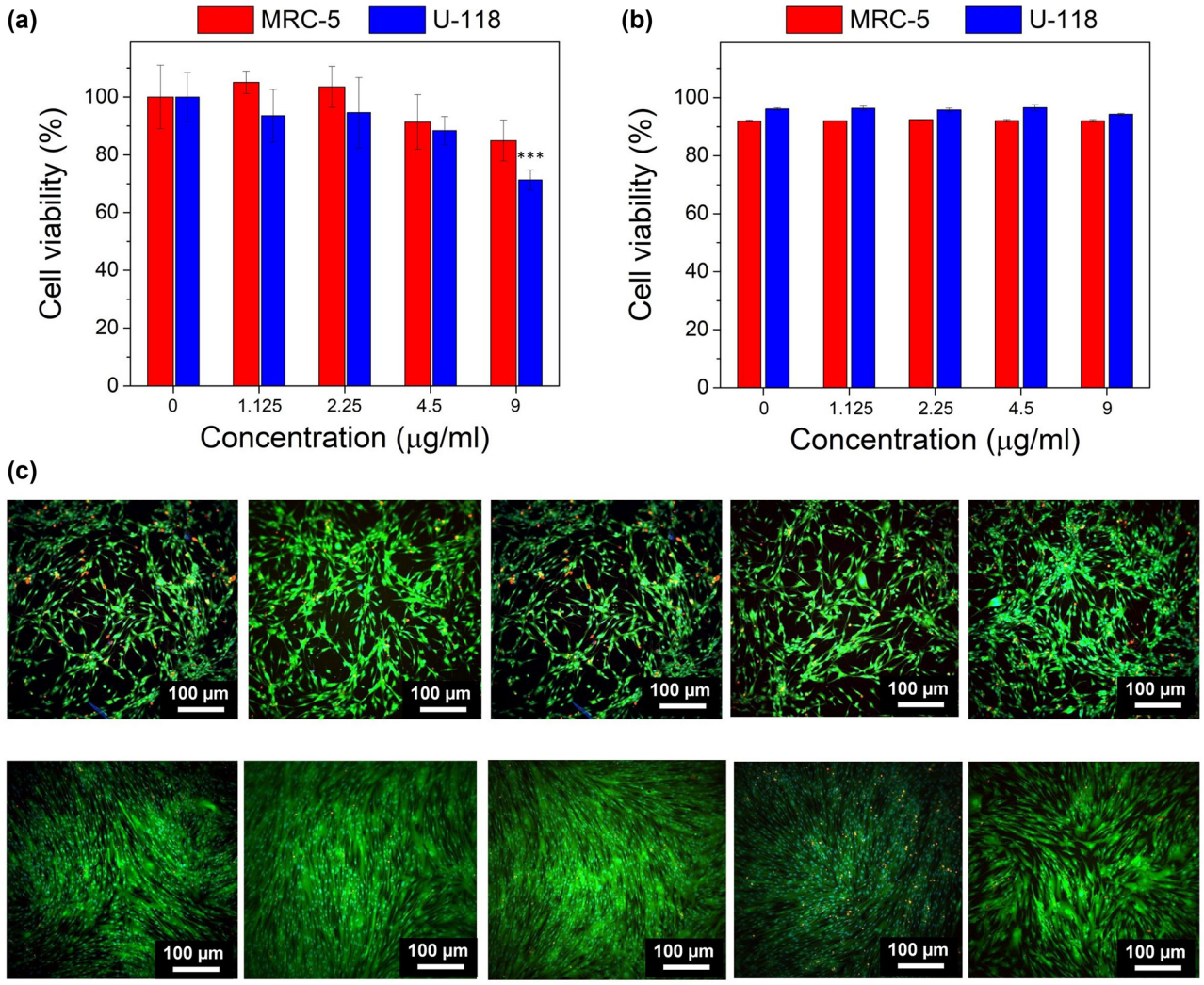

Figure 3: Proliferation level of U-118 MG and MRC-5 cells determined by WST-1 assay (a); cell viability of U-118 MG and MRC-5 cells determined by live/dead assay (b). The images of U-118 MG cells (upper row) and MRC-5 cells (lower row) obtained using IN Cell Analyzer after live/dead assay (c). Calcein-AM stains for live cell (green); PI stains for dead cells (red).

In this case, cell viability reached approximately 70% for U-118 MG cells and 80% for MRC-5 cells (Figure 3a). The results achieved using high content screening with the IN Cell Analyzer show no significant changes in the viability of U-118 MG and MRC-5 cells after incubation with PDA@DD3.0 (Figure 3b). No difference in cell viability is also confirmed by the images presented in Figure 3c. The images show mostly green signals from live cells and only a few red spots from dead cells. Therefore, PDA@DD3.0 can be considered nontoxic, because it does not negatively affect normal and cancer cells in the tested concentration range.

3.3 Chemotherapy

DOX, a model chemotherapeutic drug, is commonly used in cancer therapy. Lately, it has found application as an anticancer agent in GBM therapy [70,71]. Therefore, DOX was loaded on the PDA@DD3.0 at a 1:1 NPs to DOX ratio. UV-Vis experiments were used to specify the total amount of loaded DOX (EE% and LC%) according to the formula presented in Section 2. The calculated EE% and LC% DOX on NPs were 99% in both cases. The values are the same due to the high loading capacity of particles functionalized with dendrimers on PDA NPs surface.

The DOX release from the PDA@DD3.0 was analyzed in three different buffers mimicking the internal environment of different cellular compartments in cancer cells. The CA at pH 4.5 and 5.5 were used to recreate conditions found in lysosomes while PBS buffer pH 7.5 served as medium mimicking the physiological conditions found in the bloodstream and cells. The drug release was tested every hour for the first 6 h and then after 24 and 48 h using

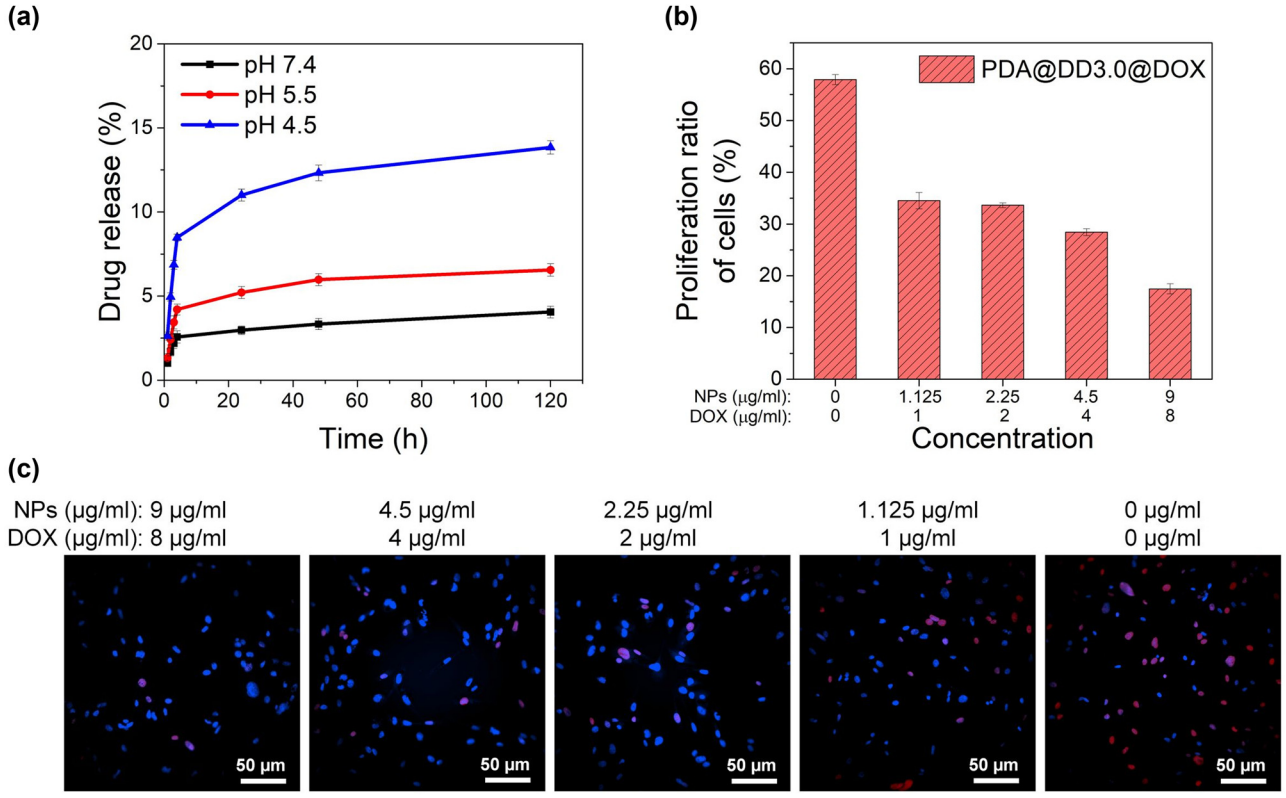

Figure 4: Release profile of DOX from PDA@DD3.0@DOX for 48 h at 37°C at different pH (a). Proliferation ratio of U-118 MG cells after incubation with PDA@DD3.0@DOX over 48 h determined by EdU cell proliferation assay (b). The images of U-118 MG cells obtained using IN Cell Analyzer after EdU cell proliferation assay (c). Hoechst 33342 stains for all nuclei (blue); Eterneon-Red 645 dye azide stains for proliferating cells (red).

a UV-Vis spectrophotometer. The results are shown in Figure 4a. It is visible that the most intense DOX release appears within the first few hours for all samples and then reaches a plateau. The highest cumulative DOX release occurs for the sample incubated in CA at pH 4.5. The lower value of cumulative release was recorded at pH 5.5 and the lowest at pH 7.4. It is known that weak non-covalent bonds can be destabilized by an acid environment and result in drug release. These experiments showed that the most efficient release occurred under conditions simulating the lowest pH in cancer cells. Moreover, the drug release phenomenon can be assigned to protonation of amine groups from PAMAM dendrimers and their electrical repulsion in acidic pH causing release of the drug from PAMAM cavities. Furthermore, the acidic conditions enhance the DOX solubility in aqua solution. The presented data confirm that DOX was released from the nanocarriers in a pH-dependent manner, as the highest release was observed at acidic pH and negligible at neutral pH.

The efficiency of drug delivery *via* synthesized nanocarriers to glioma cells was determined by EdU cell proliferation assay. For this purpose, U-118 MG cells were incubated with PDA@DD3.0@DOX at a concentration range between 9 and 1.125 μg/mL for 48 h. The percentage of proliferating U-118 MG cells was assessed using IN Cell Analyzer. In this test, modified thymidine analogue EdU was built into the newly created DNA of proliferating cells, while DOX inhibits proliferation of cells. As demonstrated in Figure 4b, treatment of glioma cells with this type of NPs is very efficient, even at the lowest concentration of NPs. The proliferation ratio for control U-118 MG cells (without DOX loaded NPs) was nearly 60% after 24 h incubation with EdU. The reduction in proliferating cell rate induced by the PDA@DD3.0@DOX was observed over the entire concentration range. For the lowest concentration of PDA@DD3.0@DOX, proliferation was reduced by almost half, while at the highest concentration we noticed a 3-fold reduction in the level of cell proliferation.

3.4 Gene therapy

To investigate the effectiveness of synthesized nanocarriers in gene therapy, we loaded double stranded RNA (dsRNA) complementary to TN-C mRNA sequence on PDA@DD3.0 *via* electrostatic interactions between positively charged surface of

PAMAM and negatively charged dsRNA. Non-covalent binding simplifies the detachment of dsRNA from the NPs and allows further downregulation of TN-C protein expression. We assessed different weight ratios between dsRNA and PDA@DD3.0 ranging from 1:1 to 30:1 to find condition for the highest loading of ATN-RNA. We evaluated the binding capacity of our material using agarose gel electrophoresis. The results are presented in Figure 5a. As can be seen, the intensity of the dsRNA signal decreases as the ratio of nanomaterials to dsRNA increases. At a ratio of 30:1, we did not observe a signal from the unbound dsRNA, indicating that the nucleic acids were fully loaded onto the nanocarrier. Here we also evaluated the binding capacity of PDA@DD3.0@DOX toward ATN-RNA. The performed experiments revealed a difference in binding efficiency between PDA@DD3.0 and PDA@DD3.0@DOX. In the case of PDA@DD3.0, the highest binding capacity was observed at a ratio of 30:1, whereas the sample with DOX required a ratio of 10:1 to fully bind ATN-RNA. This indicates that the presence of DOX in the dendrimers may improve the binding of the dsRNA to the vehicle, possibly as a result of the interaction of the dsRNA strands with DOX.

Next we also evaluated the zeta potential of the obtained materials after dsRNA binding (Figure 2f). The zeta potential value changed after the DOX loading from +40 mV to around +36 mV. Due to the location of DOX inside the dendrimer structure, the reduction in surface charge is minimal. The electrokinetic potential of the final product after dsRNA binding (PDA@DD3.0@DOX@ATN-RNA) at a ratio of 30:1 (NPs to dsRNA wt/wt ratio) was around −20 mV which is a result of negatively charged dsRNA attached to the nanoparticles.

We then tested the ability of our material for RNAi therapy by incubating U-118 MG cells with PDA@DD3.0@DOX@ATN-RNA carrying different concentrations of ATN-RNA (12.5, 25, 50, and 100 nM) to reduce expression of TN-C transcript. We used PDA@DD3.0@DOX at 30:1 material to ATN-RNA wt/wt ratio. Then, the qRT-PCR was conducted after 24 h of cell incubation with the particles to determine the expression level of TN-C. The silencing of TN-C mRNA expression was investigated by comparing PDA@DD3.0@DOX NPs without dsRNA. As demonstrated in Figure 5b, the decrease in the TN-C expression level was observed at higher concentrations of used material. TN-C level decreased from 80% at 50 nM dsRNA to 70% for cells treated with 100 nM dsRNA, while this effect was not visible at 25 nM. There is no apparent alteration in TN-C expression in the case of dsRNA free NPs. It can therefore be concluded that under the conditions used, our carrier was able to deliver dsRNA and downregulate TN-C in U-118 MG cells at concentrations higher than 50 nM dsRNA.

3.5 Photothermal properties and therapy

The photothermal characteristics of pristine PDA NPs were analyzed by temperature measurement at 10 s intervals

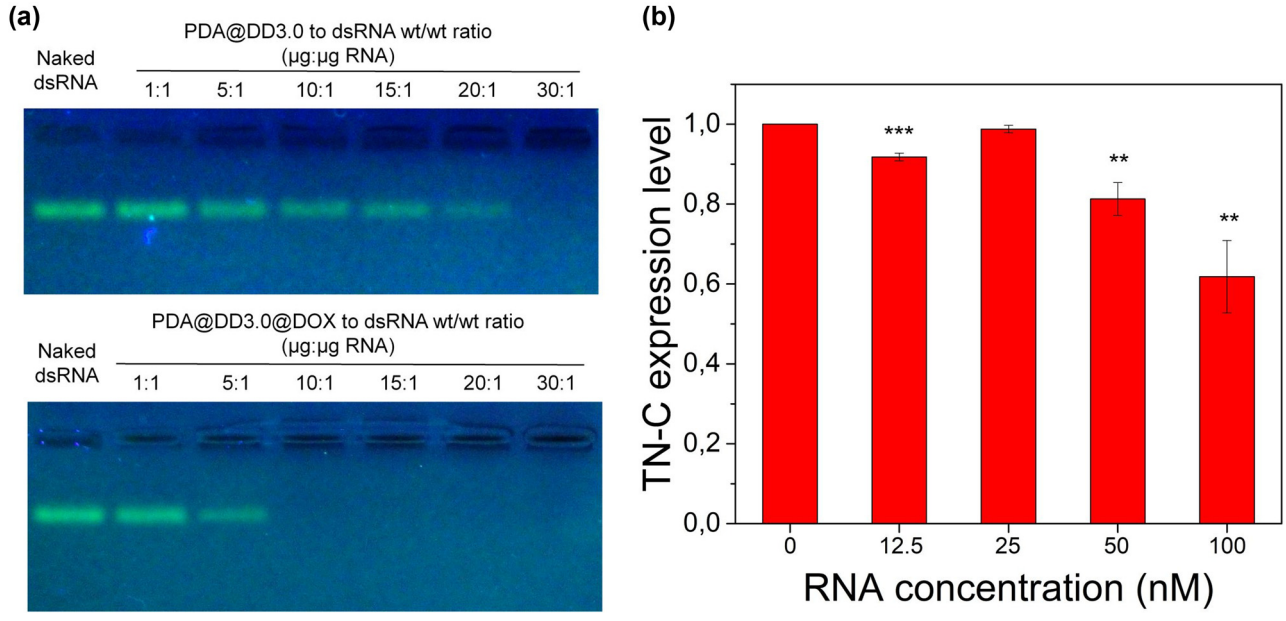

Figure 5: Agarose gel electrophoresis of PDA@DD3.0 and PDA@DD3.0@DOX complexes with dsRNA at different mass ratios (a). Quantification of mRNA TN-C expression level on U-118 MG cells after incubation with PDA@DD3.0@DOX@ATN-RNA (b).

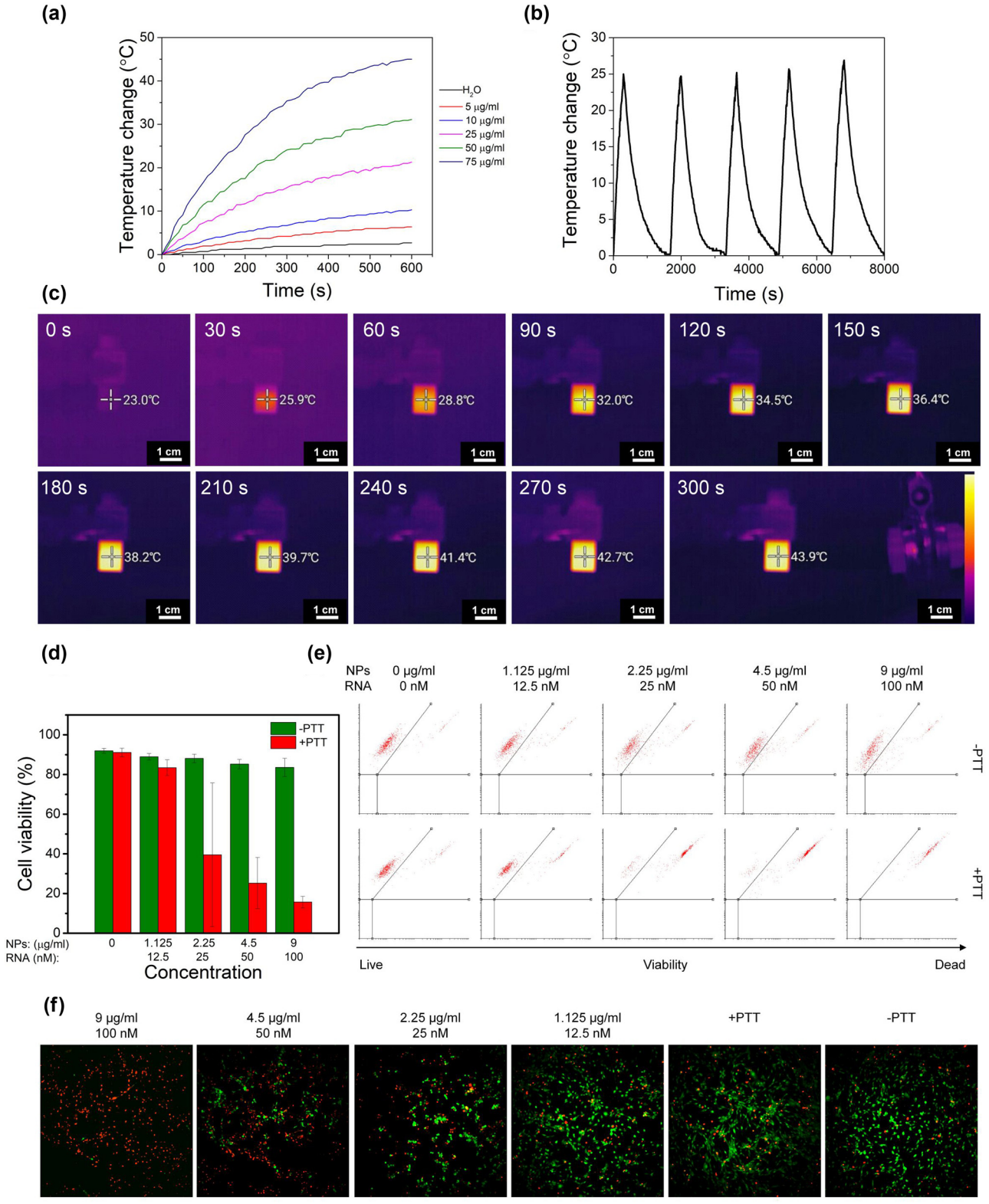

Figure 6: Temperature increase (a), photothermal stability (b), and thermographic camera images (c) of the PDA NPs solution after irradiation with 808 nm laser beam. Cell viability (d) calculated from flow cytometry dot plots (e) and images obtained using IN Cell Analyzer of U-118 MG cells incubated with PDA@DD3.0@DOX@ATN-RNA with (+PTT) and without (−PTT) 808 nm laser irradiation using live/dead assay (f). Calcein-AM staining for living cells (green); PI staining for dead cells (red).

during 10 min of irradiation with laser light at 808 nm wavelength and a laser power of 3 W (Figure 6a). The temperature change of the solution varied in a concentration-dependent manner. The most significant temperature growth is demonstrated within the first few minutes of irradiation and then slowly saturates. The highest temperature change of the NPs solution was obtained at 100 µg/mL particles concentration subjected to NIR laser irradiation. The recorded temperature change was 47°C. As observed in the graph, the temperature change in the control sample is hardly visible. Another critical aspect of PTT is the stability of the material used to rise the temperature. The photostability measurements showed that these NPs could be applied in at least five on/off laser irradiation cycles, which confirms that this material is highly stable over time (Figure 6b). We also imaged temperature change using a thermographic camera. The camera focus was aimed at the center of the cuvette containing 50 µg/mL of PDA NPs in water. Images were taken every 30 s during 5 min of exposure to laser light. The temperature rise is represented based on the color intensity according to the thermal scale, and the specific temperature value in the cuvette is also demonstrated numerically in the photo (Figure 6c). The maximum value after 300 s corresponds to the value shown in Figure 6a. The data obtained from both techniques were consistent.

Finally, the efficiency of PTT using live/dead cell viability assay was assessed. To avoid the influence of DOX on cell survivability, U-118 MG cells were incubated for 24 h with PDA@DD3.0@ATN-RNA in the concentration range from 9 to 1.125 µg/mL, and then irradiated with a laser beam at 808 nm. The number of live and dead cells was measured by flow cytometry after another 24 h (Figure 6d and e). Data analysis revealed that there was no difference in cell viability compared to control cells when the cells were not irradiated with laser beam. However, after laser irradiation at the two highest concentrations, we noticed a significant decrease in cell viability. This confirmed the high efficacy of PTT, which at the highest concentration reduced the number of living cells to 20%. The PTT effect is also demonstrated as microscopic images (Figure 6f).

3.6 Imaging

Confocal imaging was carried out to demonstrate the release of DOX from PDA@DD3.0@DOX@ATN-RNA inside U-118 MG cells. Cells were incubated with PDA@DD3.0@DOX@ATN-RNA at concentrations of 9 µg/mL (with respect to NPs concentration) for 4 h. After this time, the cells were fixed and photos were taken using a fluorescence microscope. As it is observed in Figure 7, high uptake efficacy of PDA@DD3.0@DOX@ATN-RNA resulting in DOX release (red color) after 4 h of incubation with U-118 MG cells was noticed. We also showed cell nuclei stained with Hoechst 33342 dye (blue). Combining the acquired images revealed that DOX enters the cell and accumulates in the nuclear region. Thus, these results proved that DOX is able to provide effective chemotherapeutic therapy (as shown in Figure 3b) by intercalating in the DNA structure, inhibiting cell proliferation.

4 Conclusion

In this study, we demonstrated that PDA-based nanocarriers are promising drug/gene delivery platforms that can find application in combined anticancer therapies. The size of PDA NPs can be easily controlled by the concentration of NaOH in the solution. The use of PAMAM dendrimers on PDA NPs allows for high DOX loading efficiency and effective anti-TN-C RNA binding. The biggest cumulative release of DOX from PDA@DD3.0 is observed at pH 4.5, analogously to the environment inside cancer cells. The synthesized material possesses strong photothermal characteristics sufficient for PTT. PDA NPs are characterized by high PT stability within five on/off irradiation cycles, which confirms that they could be irradiated repeatedly. Confocal imaging proves effective DOX delivery using PDA@DD3.0 NPs into U-118 MG cells. DOX accumulation is demonstrated near the nuclei. The obtained PDA NPs do not show significant cytotoxic effects in normal MRC-5 and cancer U-118 MG

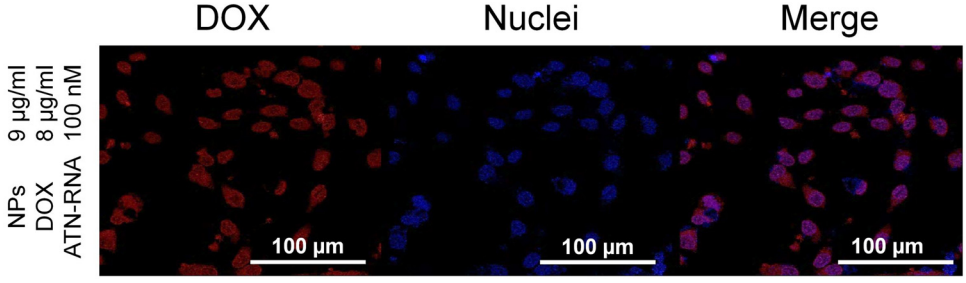

Figure 7: Confocal laser scanning microscopy images demonstrating the presence of DOX delivered by NPs in U-118 MG cells. Imaging was conducted after 4 h of incubation with PDA@DD3.0@DOX@ATN-RNA at a concentration of 9 µg/mL. Hoechst 33342 staining for nuclei (blue); DOX (red).

cells after incubation for 48 h. The chemotherapeutic effect of PDA@DD3.0@DOX is confirmed by reducing proliferation of U-118 MG cells. The phototherapeutic effect of PDA@DD3.0 NPs is demonstrated by a decrease in the viability of U-118 MG cells, especially at the highest concentration of NPs, whereas the gene therapy effect of PDA@DD3.0 NPs is proved by a decrease in the expression of TN-C in U-118 MG cells.

Funding information: The research was financially supported by the National Science Centre (NCN) under project nos UMO-2018/31/D/ST8/02434 and UMO-2018/21/B/ST8/02460. K.Ż. would like to express her gratitude for the National Centre for Research and Development – project no. DWM/WPC2/285/2020 and the Program POWR.03.02.00-00-I032/16.

Author contributions: Klaudia Żebrowska: investigation, methodology, visualization, and writing – original draft. Małgorzata Grabowska – investigation and writing – review and editing. Emerson Coy – investigation and writing – review and editing. Katarzyna Rolle: methodology and writing – review and editing. Radosław Mrówczyński: conceptualization, methodology, writing – review and editing, and funding acquisition. Bartosz F. Grześkowiak: conceptualization, investigation, methodology, visualization, writing – original draft, and funding acquisition. All authors have accepted responsibility for the entire content of this manuscript and approved its submission.

Conflict of interest: The authors state no conflict of interest.

References

[1] Jovčevska I, Kočevar N, Komel R. Glioma and glioblastoma – how much do we (not) know? Mol Clin Oncol. 2013;1(6):935–41.
[2] Bicker J, Alves G, Fortuna A, Falcão A. Blood-brain barrier models and their relevance for a successful development of CNS drug delivery systems: a review. Eur J Pharm Biopharm. 2014;87(3):409–32.
[3] Mohammed S, Dinesan M, Ajayakumar T. Survival and quality of life analysis in glioblastoma multiforme with adjuvant chemoradiotherapy: a retrospective study. Rep Pract Oncol Radiother. 2022;27(6):1026–36.
[4] Lee SY. Temozolomide resistance in glioblastoma multiforme. Genes Dis. 2016;3(3):198–210.
[5] Mitusova K, Peltek OO, Karpov TE, Muslimov AR, Zyuzin MV, Timin AS. Overcoming the blood–brain barrier for the therapy of malignant brain tumor: current status and prospects of drug delivery approaches. J Nanobiotechnol. 2022;20(1):412.
[6] Harder BG, Blomquist MR, Wang J, Kim AJ, Woodworth GF, Winkles JA, et al. Developments in Blood-Brain Barrier Penetrance and Drug Repurposing for Improved Treatment of Glioblastoma. Front Oncol. 2018;8:462.
[7] Park SH, Kim MJ, Jung HH, Chang WS, Choi HS, Rachmilevitch I, et al. One-Year Outcome of Multiple Blood-Brain Barrier Disruptions With Temozolomide for the Treatment of Glioblastoma. Front Oncol. 2020;10:1663.
[8] Seeta Rama Raju G, Benton L, Pavitra E, Yu JS. Multifunctional nanoparticles: recent progress in cancer therapeutics. Chem Commun (Camb). 2015;51(68):13248–59.
[9] Kim D, Shin K, Kwon SG, Hyeon T. Synthesis and biomedical applications of multifunctional nanoparticles. Adv Mater. 2018;30(49):e1802309.
[10] Parvanian S, Mostafavi SM, Aghashiri M. Multifunctional nanoparticle developments in cancer diagnosis and treatment. Sens Bio-Sens Res. 2017;13:81–7.
[11] Mrówczyński R. Polydopamine-based multifunctional (nano)materials for cancer therapy. ACS Appl Mater Interfaces. 2018;10(9):7541–61.
[12] Bao G, Mitragotri S, Tong S. Multifunctional nanoparticles for drug delivery and molecular imaging. Annu Rev Biomed Eng. 2013;15:253–82.
[13] McCarthy JR, Weissleder R. Multifunctional magnetic nanoparticles for targeted imaging and therapy. Adv Drug Deliv Rev. 2008;60(11):1241–51.
[14] Ribovski L, Hamelmann NM, Paulusse JMJ. Polymeric nanoparticles properties and brain delivery. Pharmaceutics. 2021;13(12):2045.
[15] Liu Z, Ji X, He D, Zhang R, Liu Q, Xin T. Nanoscale drug delivery systems in glioblastoma. Nanoscale Res Lett. 2022;17(1):27.
[16] Gregory JV, Kadiyala P, Doherty R, Cadena M, Habeel S, Ruoslahti E, et al. Systemic brain tumor delivery of synthetic protein nanoparticles for glioblastoma therapy. Nat Commun. 2020;11(1):5687.
[17] Marei HE. Multimodal targeting of glioma with functionalized nanoparticles. Cancer Cell Int. 2022;22(1):265.
[18] Xin Y, Huang M, Guo WW, Huang Q, Zhang LZ, Jiang G. Nano-based delivery of RNAi in cancer therapy. Mol Cancer. 2017;16(1):134.
[19] Gao H, Cheng R, A. Santos H. Nanoparticle-mediated siRNA delivery systems for cancer therapy. View. 2021;2(3):20200111.
[20] Swaminathan G, Shigna A, Kumar A, Byroju VV, Durgempudi VR, Dinesh Kumar L. RNA interference and nanotechnology: A promising alliance for next generation cancer therapeutics. Front Nanotechnol. 2021;3:694838.
[21] Lozada-Delgado EL, Grafals-Ruiz N, Vivas-Mejía PE. RNA interference for glioblastoma therapy: Innovation ladder from the bench to clinical trials. Life Sci. 2017;188:26–36.
[22] Teng X-Q, Qu J, Li G-H, Zhuang H-H, Qu Q. Small interfering RNA for gliomas treatment: Overcoming hurdles in delivery. Front Cell Dev Biol. 2022;10:824299.
[23] Harrison C. RNAi-based nanoparticles zap glioblastoma. Nat Rev Drug Discov. 2014;13(1):20.
[24] Kozielski KL, Ruiz-Valls A, Tzeng SY, Guerrero-Cázares H, Rui Y, Li Y, et al. Cancer-selective nanoparticles for combinatorial siRNA delivery to primary human GBM *in vitro* and *in vivo*. Biomaterials. 2019;209:79–87.
[25] Grabowska M, Grześkowiak BF, Szutkowski K, Wawrzyniak D, Głodowicz P, Barciszewski J, et al. Nano-mediated delivery of double-stranded RNA for gene therapy of glioblastoma multiforme. PLOS One. 2019;14(3):e0213852.
[26] Gulcher JR, Nies DE, Alexakos MJ, Ravikant NA, Sturgill ME, Marton LS, et al. Structure of the human hexabrachion (tenascin) gene. Proc Natl Acad Sci U S A. 1991;88(21):9438–42.

[27] Castaños-Velez E, Biberfeld P, Patarroyo M. Extracellular matrix proteins and integrin receptors in reactive and non-reactive lymph nodes. Immunology. 1995;86(2):270–8.
[28] Orend G, Chiquet-Ehrismann R. Tenascin-C induced signaling in cancer. Cancer Lett. 2006;244(2):143–63.
[29] Fukushima T, Tezuka T, Shimomura T, Nakano S, Kataoka H. Silencing of insulin-like growth factor-binding protein-2 in human glioblastoma cells reduces both invasiveness and expression of progression-associated gene CD24. J Biol Chem. 2007;282(25):18634–44.
[30] Tchirkov A, Khalil T, Chautard E, Mokhtari K, Véronèse L, Irthum B, et al. Interleukin-6 gene amplification and shortened survival in glioblastoma patients. Br J Cancer. 2007;96(3):474–6.
[31] Nakada M, Nakada S, Demuth T, Tran NL, Hoelzinger DB, Berens ME. Molecular targets of glioma invasion. Cell Mol Life Sci. 2007;64(4):458–78.
[32] Pas J, Wyszko E, Rolle K, Rychlewski L, Nowak S, Zukiel R, et al. Analysis of structure and function of tenascin-C. Int J Biochem Cell Biol. 2006;38(9):1594–602.
[33] Sarkar S, Nuttall RK, Liu S, Edwards DR, Yong VW. Tenascin-C stimulates glioma cell invasion through matrix metalloproteinase-12. Cancer Res. 2006;66(24):11771–80.
[34] Zagzag D, Shiff B, Jallo GI, Greco MA, Blanco C, Cohen H, et al. Tenascin-C promotes microvascular cell migration and phosphorylation of focal adhesion kinase. Cancer Res. 2002;62(9):2660–8.
[35] Wang Y, Sun Y, Geng N, Zheng M, Zou Y, Shi B. A biomimetic nanomedicine targets orthotopic glioblastoma by combinatorial co-delivery of temozolomide and a methylguanine-DNA methyltransferase inhibitor. Adv Ther. 2022;5(12):2200095.
[36] Mujokoro B, Adabi M, Sadroddiny E, Adabi M, Khosravani M. Nanostructures mediated co-delivery of therapeutic agents for glioblastoma treatment: A review. Mater Sci Eng C Mater Biol Appl. 2016;69:1092–102.
[37] Zhao M, van Straten D, Broekman MLD, Préat V, Schiffelers RM. Nanocarrier-based drug combination therapy for glioblastoma. Theranostics. 2020;10(3):1355–72.
[38] Kaneshiro TL, Lu ZR. Targeted intracellular codelivery of chemotherapeutics and nucleic acid with a well-defined dendrimer-based nanoglobular carrier. Biomaterials. 2009;30(29):5660–6.
[39] Cheng D, Cao N, Chen J, Yu X, Shuai X. Multifunctional nanocarrier mediated co-delivery of doxorubicin and siRNA for synergistic enhancement of glioma apoptosis in rat. Biomaterials. 2012;33(4):1170–9.
[40] Jaque D, Martínez Maestro L, del Rosal B, Haro-Gonzalez P, Benayas A, Plaza JL, et al. Nanoparticles for photothermal therapies. Nanoscale. 2014;6(16):9494–530.
[41] Chen J, Ning C, Zhou Z, Yu P, Zhu Y, Tan G, et al. Nanomaterials as photothermal therapeutic agents. Prog Mater Sci. 2019;99:1–26.
[42] Kim M, Lee J-H, Nam J-M. Plasmonic photothermal nanoparticles for biomedical applications. Adv Sci (Weinh). 2019;6(17):1900471.
[43] Doughty ACV, Hoover AR, Layton E, Murray CK, Howard EW, Chen WR. Nanomaterial applications in photothermal therapy for cancer. Mater (Basel). 2019;12(5):799.
[44] Mona LP, Songca SP, Ajibade PA. Synthesis and encapsulation of iron oxide nanorods for application in magnetic hyperthermia and photothermal therapy. Nanotechnol Rev. 2022;11(1):176–90.
[45] Haghighat Bayan MA, Dias YJ, Rinoldi C, Nakielski P, Rybak D, Truong YB, et al. Near-infrared light activated core-shell electrospun nanofibers decorated with photoactive plasmonic nanoparticles for on-demand smart drug delivery applications. J Polym Sci. 2023;61(7):521–33.
[46] Yan B-Y, Cao Z-K, Hui C, Sun T-C, Xu L, Ramakrishna S, et al. MXene@Hydrogel composite nanofibers with the photo-stimulus response and optical monitoring functions for on-demand drug release. J Colloid Interface Sci. 2023;648:963–71.
[47] Zheng P, Ding B, Li G. Polydopamine-incorporated nanoformulations for biomedical applications. Macromol Biosci. 2020;20(12):e2000228.
[48] Jin A, Wang Y, Lin K, Jiang L. Nanoparticles modified by polydopamine: Working as "drug" carriers. Bioact Mater. 2020;5(3):522–41.
[49] Chen R, Zhu C, Fan Y, Feng W, Wang J, Shang E, et al. Polydopamine-based multifunctional platform for combined photothermal therapy, chemotherapy, and immunotherapy in malignant tumor treatment. ACS Appl Bio Mater. 2019;2(2):874–83.
[50] Wang H, Williams GR, Xie X, Wu M, Wu J, Zhu L. Stealth polydopamine-based nanoparticles with red blood cell membrane for the chemo-photothermal therapy of cancer. ACS Appl Bio Mater. 2020;3(4):2350–9.
[51] Liu G, Gao N, Zhou Y, Nie J, Cheng W, Luo M, et al. Polydopamine-based “four-in-one” versatile nanoplatforms for targeted dual chemo and photothermal synergistic cancer therapy. Pharmaceutics. 2019;11(10):507.
[52] Mrówczyński R, Grześkowiak BF. Biomimetic catechol-based nanomaterials for combined anticancer therapies. In: Jana S, Jana S, editors. Nanoengineering of biomaterials. Weinheim, Germany: Wiley-VCH GmbH; 2022. p. 145–80.
[53] Lee H, Dellatore SM, Miller WM, Messersmith PB. Mussel-inspired surface chemistry for multifunctional coatings. Science (New York, NY). 2007;318(5849):426–30.
[54] Ryu JH, Messersmith PB, Lee H. Polydopamine surface chemistry: A decade of discovery. ACS Appl Mater Interfaces. 2018;10(9):7523–40.
[55] Yue Y, Zhao X. Melanin-like nanomedicine in photothermal therapy applications. Int J Mol Sci. 2021;22(1):399.
[56] Tian L, Li X, Ji H, Yu Q, Yang M, Guo L, et al. Melanin-like nanoparticles: advances in surface modification and tumour photothermal therapy. J Nanobiotechnology. 2022;20(1):485.
[57] Mrówczyński R, Nan A, Turcu R, Leistner J, Liebscher J, Polydopamine A. Versatile coating for surface-initiated ring-opening polymerization of lactide to polylactide. Macromol Chem Phys. 2015;216(2):211–7.
[58] Grześkowiak BF, Maziukiewicz D, Kozłowska A, Kertmen A, Coy E, Mrówczyński R. Polyamidoamine dendrimers decorated multifunctional polydopamine nanoparticles for targeted chemo- and photothermal therapy of liver cancer model. Int J Mol Sci. 2021;22(2):738.
[59] Jędrzak A, Grześkowiak BF, Coy E, Wojnarowicz J, Szutkowski K, Jurga S, et al. Dendrimer based theranostic nanostructures for combined chemo- and photothermal therapy of liver cancer cells *in vitro*. Colloids Surf B Biointerfaces. 2019;173:698–708.
[60] Maziukiewicz D, Grześkowiak BF, Coy E, Jurga S, Mrówczyński R. NDs@PDA@ICG conjugates for photothermal therapy of glioblastoma multiforme. Biomim (Basel). 2019;4(1):3.
[61] Maziukiewicz D, Mrówczyński R, Jurga S, Grześkowiak BF. Laser synthesized nanodiamonds with hyper-branched polyglycerol and polydopamine for combined imaging and photothermal treatment. Diam Relat Mater. 2022;128:109308.

[62] Wu H, Wei M, Xu Y, Li Y, Zhai X, Su P, et al. PDA-based drug delivery nanosystems: A potential approach for glioma treatment. Int J Nanomed. 2022;17:3751–75.
[63] Ho CC, Ding SJ. The pH-controlled nanoparticles size of polydopamine for anti-cancer drug delivery. J Mater Sci Mater Med. 2013;24(10):2381–90.
[64] Jędrzak A, Grześkowiak BF, Golba K, Coy E, Synoradzki K, Jurga S, et al. Magnetite nanoparticles and spheres for chemo- and photothermal therapy of hepatocellular carcinoma *in vitro*. Int J Nanomed. 2020;15:7923–36.
[65] Bernsmann F, Frisch B, Ringwald C, Ball V. Protein adsorption on dopamine–melanin films: Role of electrostatic interactions inferred from ζ-potential measurements versus chemisorption. J Colloid Interface Sci. 2010;344(1):54–60.
[66] Tejido-Rastrilla R, Ferraris S, Goldmann WH, Grünewald A, Detsch R, Baldi G, et al. Studies on cell compatibility, antibacterial behavior, and zeta potential of Ag-containing polydopamine-coated bioactive glass-ceramic. Mater (Basel). 2019;12(3):500.
[67] Fu J, Chen Z, Wang M, Liu S, Zhang J, Zhang J, et al. Adsorption of methylene blue by a high-efficiency adsorbent (polydopamine microspheres): Kinetics, isotherm, thermodynamics and mechanism analysis. J Chem Eng. 2015; 259:53–61.
[68] Su L, Yu Y, Zhao Y, Liang F, Zhang X. Strong antibacterial polydopamine coatings prepared by a shaking-assisted method. Sci Rep. 2016;6(1):24420.
[69] Ball V. Impedance spectroscopy and zeta potential titration of dopa-melanin films produced by oxidation of dopamine. Colloids Surf A: Physicochem Eng Asp. 2010;363(1):92–7.
[70] Matcovschii V, Lisii D, Gudumac V, Dorosenco S. Selective interstitial doxorubicin for recurrent glioblastoma. Clin Case Rep. 2019;7(12):2520–5.
[71] Norouzi M, Yathindranath V, Thliveris JA, Kopec BM, Siahaan TJ, Miller DW. Doxorubicin-loaded iron oxide nanoparticles for glioblastoma therapy: a combinational approach for enhanced delivery of nanoparticles. Sci Rep. 2020;10(1):11292.